Title: Dysregulation of the Leukocyte Signaling Landscape during Acute COVID-19

Isaiah R. Turnbull[1], Anja Fuchs[1], Kenneth E. Remy[4], Michael P. Kelly[3], Elfaridah P. Frazier[3], Sarbani Ghosh[1], Shin-Wen Chang[1], Monty Mazer[2], Annie Hess[1], Jennifer Leonard[1], Mark Hoofnagle[1], Marco Colonna[5] and Richard S. Hotchkiss[1]

Departments of Surgery[1], Anesthesia[2], Orthopedic Surgery[3], Pediatrics[4], Pathology and Immunology[5], Washington University School of Medicine, 660 South Euclid Avenue, St. Louis, MO 63110, USA

Corresponding Author:

Isaiah R. Turnbull, MD, PhD

Washington University School of Medicine

Department of Surgery

Campus Box 8109

660S Euclid Avenue

St Louis, MO 63110

Phone: 314-263-9347

Fax: 314-3629345

iturnbull@wustl.edu

Abstract: The global COVID-19 pandemic has claimed the lives of more than 450,000 US citizens. Dysregulation of the immune system underlies the pathogenesis of COVID-19, with inflammation mediated local tissue injury to the lung in the setting of suppressed systemic immune function. To define the molecular mechanisms of immune dysfunction in COVID-19 we utilized a systems immunology approach centered on the circulating leukocyte phosphoproteome measured by mass cytometry. COVID-19 is associated with wholesale activation of a broad set of signaling pathways across myeloid and lymphoid cell populations. STAT3 phosphorylation predominated in both monocytes and T cells and was tightly correlated with circulating IL-6 levels. High levels of STAT3 phosphorylation was associated with decreased markers of myeloid cell maturation/activation and decreased ex-vivo T cell IFN-gamma production, demonstrating that during COVID-19 dysregulated cellular activation is associated with suppression of immune effector cell function. Collectively, these data reconcile the systemic inflammatory response and functional immunosuppression induced by COVID-19 and suggest STAT3 signaling may be the central pathophysiologic mechanism driving immune dysfunction in COVID-19.

Introduction:

In December of 2019, COVID-19 syndrome emerged in the Wuhan province of Western China. The novel corona virus SARS-CoV2 was rapidly recognized as the etiologic agent of COVID-19. Over the last 12 months, a combination of facile respiratory transmission, a high incidence asymptomatic carriers, and an immunologically naïve population have synergized to foment a global pandemic that has resulted in over 100 million cases of COVID-19 worldwide[1]. There have been more than 450,000 deaths in the US alone [2], comprising more than one out of a thousand US citizens, consistent with reports of an infection mortality rate ranging from 0.3-1%. SARS-CoV2 infectious disease spans the clinical spectrum from asymptomatic carriage to life-threatening critical illness. Approximately 5% of infected persons experience severe COVID-19 disease, clinically manifest as a viral sepsis syndrome defined by a dysregulated immune-inflammatory response and new onset organ failure[3, 4, 5, 6, 7]. The described pathophysiology of severe COVID-19 recapitulates the last 30 years of sepsis research: a fulminant cytokine dyscrasia overlying functional immunosuppression, coagulopathy and thrombosis-mediated organ damage, neurologic complications including delirium and ICU psychosis, and a risk of long-term, persistent illness[8].

Early reports characterized COVID19 as driven by a cytokine storm syndrome. This hypothesis was based on early data demonstrating elevated levels canonical inflammatory mediators such as IL-6 and CXCL-10, suggesting that a cytokine-induced systemic inflammatory response was driving the pathophysiology of the disease[9, 10, 11, 12]. Subsequent studies elucidated a more complex immunophenotype for COVID-19, with profound changes in both myeloid and lymphoid leukocyte populations including mobilization of immature myeloid cells from the bone-marrow[13, 14, 15], an increase in circulating B-cell plasmablasts and

an overall lymphopenia including CD4, CD8 and invariant (γδ) T cells. These changes in leukocyte populations were associated with an increase in immature “low-density” neutrophils population, an increase in immunosuppressive HLA-DR^{lo} monocytes and a shift toward a broadly “activated” T cell phenotype, which based on correlation analysis were driven by the circulating inflammatory cytokinemia[16, 17, 18, 19]. Further functional studies directly assessing leukocyte function demonstrated that like severe sepsis, severe COVID-19 is associated with an overall suppressed immunotype[20, 21]. Our group reported that severe COVID-19 was associated with defects in T cell production of IFN-gamma and monocyte TNF-alpha production[22] and others reported weak CD8 T cell responses to COVID-19 antigen and impaired DC function[23]. Taken together, the data present a complex picture of immune dysfunction during COVID-19 with high levels of circulating inflammatory mediators, neutrophilia and partial T cell activation, but functional immunosuppression.

To better characterize the effect of COVID-19 on the immune system we sought to define the intracellular signaling milieu of circulating leukocytes during acute COVID-19. We deployed a mass cytometry assay to measure the leukocyte phosphoproteome in moderate and severely ill COVID-19 patients and correlated changes in the intracellular signaling landscape with circulating cytokine levels and measures of cellular activation and function. We found that COVID-19 is associated with a significant dysregulation of the leukocyte signaling landscape, with broad based increase in signaling phosphoprotein levels in all circulating leukocyte populations tested. In myeloid cell populations, surface markers of activation and maturation were negatively correlated with activation of ERK, STAT3, STAT1 and CREB. Similarly, in CD4 and CD8 T cells high levels of STAT3 phosphorylation was correlated with defects in ex-vivo IFN-γ production. Taken together these data begin to reconcile the COVID-19 induced inflammatory cytokinemia with the well described functional immunosuppression documented in critically ill COVID-19 patients[9, 14, 17, 18, 21, 22, 23, 24, 25, 26, 27].

Methods:

Study Design and Recruitment. Patients were recruited from April 2020-November 2020 at Missouri Baptist Medical Center and Barnes-Jewish Hospital. Symptomatic patients over age 18 with a pending, clinically indicated SARS-CoV2 nasopharyngeal PCR test were approached for consent. Subjects with a subsequent negative COVID-19 test were excluded. Blood samples were obtained from peripheral venipuncture or from existing venous catheters. All blood samples included in this analysis were obtained within 72 hours of hospital presentation. 63 subjects are included. 43 subjects had severe COVID-19 disease requiring admission to the intensive care unit (ICU). 20 subjects had moderate disease requiring inpatient hospitalization but no ICU care. Demographic and clinical data was abstracted from the electronic medical record. Concurrently a cohort of healthy donor patients was recruited. Healthy donors had no self-reported acute illness or history of chronic infection, autoimmune disease, malignancy or organ transplantation. For all samples, blood was collected into heparinized vacutainers stored at room temperature. All samples were processed within 4 hours of phlebotomy. Study protocols were approved by the Washington University in St. Louis Institutional Review Board (approval # 202003085) or the Missouri Baptists Medical Center Institutional Review Board (approval # 1132).

Sample Processing, Staining and Mass Cytometry Acquisition. 1mL of whole blood was mixed with 1.4 volumes of Proteomic Stabilizer (Smart Tube Inc, San Carlos, CA), incubated at room temperature for 10 minutes, then stored at -80° Celsius until analysis. At the time of analysis samples were thawed and red blood cells were lysed using Thaw-Lyse buffer (Smart Tube Inc, San Carlos, CA) and permeabilized for staining with MaxPar Barcoding Perm Buffer (Fluidigm Inc, San Francisco, CA) following manufacturers' protocols. Cell numbers were enumerated and 3x10^6 cells were transferred for staining. Individual

samples were first barcoded by incubation with Cell-ID 20-Plex Pd Barcoding Kit (Fluidigm) following manufacturers protocol. Up to 10 samples were pooled, washed x2 with CyFACS then resuspended in 0.5 mL CyFACS. Fc Receptors were blocked by adding 45 uL TruStain FcX (Biolegend) at RT for 10 min. Surface antibody cocktail was then added (see Extended Data Table 1) and sample incubated for 1 hour on ice. Cells were then washed in 10 mL of CyFACS buffer x1.

For intracellular staining cell pellet was resuspended in -20° C methanol to a final concentration of 5x10^6 cells/ml and incubated at -20° C for 30 min, then washed 2x in 10 mL of ice-cold CyFACS buffer. Cells were resuspended in 1mL CyFACS buffer then incubated for 60 minutes on ice with intracellular antibody cocktail (see Extended Data Table 1). Cells were washed x2 with 10 mL CyFACS buffer, then resuspended in FACS buffer containing 2% PFA and Cell ID Intercalator Solution (Fluidigm, San Francisco, CA) following manufacturers protocol for DNA staining.

Cells were analyzed on a Fluidigm CyTOF 2 Mass Cytometer. Samples were first resuspended in water+10% EQ Four Element Calibration Beads (Fluidigm) then acquired with an event rate of ~500 events/sec. CyTOF data were analyzed using the FlowJo software platform (BD, Franklin Lakes, NJ).

All antibodies were commercially conjugated to heavy metal isotopes except for clones B1.1, WM53, ICRF44, VI-PL2 and 7C9. For these clones unconjugated antibodies were purchased and conjugated using MAXPAR Antibody Labeling Kit (Fluidigm, San Francisco, CA) following manufacturers protocols.

Soluble Molecule Determination. For plasma studies, cellular elements of whole blood were pelleted by centrifugation at 1000 xg for 7 minutes at room temperature; soluble phase was aspirated, aliquoted and stored at -80° C. Cytokine and chemokine levels were determined by multiplex bead array (Cytokine

Human Magnetic 35 Plex Panel, ThermoFisher Scientific) following manufacturers protocol. Samples were acquired on a Luminex FLEXMAP 3D instrument system.

Enzyme-linked Immunospot (ELISpot) assay. Peripheral blood mononuclear cells (PBMCs) were isolated from 5 mL fresh whole blood as previously described[22]. Total number of PBMCs was determined using a Vi-Cell™ viability analyzer (Beckman Coulter, Brea, CA, USA). Flow cytometry was performed for cell typing, staining for CD3, CD4, CD8 and CD14. Detection of *ex vivo* production of IFN-ɣ was assessed by ELISpot using precoated plates (ImmunoSpot by Cellular technology Limited (CTL), Cleveland, OH, USA) as per manufacturers protocols. Cells were incubated in serum-free media (CTL) with 500 ng/mL of anti-CD3 (Bio-legend clone HIT3a) with 2.5 µg/mL of anti-CD28 (Bio-legend clone CD28.2) antibodies in a total well volume of 200 µg for 2.5 x 10^4 PBMCs. Following overnight incubation at 37° C in 5% CO_2, biotinylated detection antibody, streptavidin bound alkaline phosphatase and developer solution were applied as per manufacturer instructions. ELISpot analysis was performed using a CTL series 6 ImmunoSpot Universal Analyzer with Immunospot 7.0 professional software (CTL Analyzers, Shaker Heights, OH).

Data Analysis. Cell number, cell frequency, subpopulation frequency and signal intensities were compared across healthy, moderate COVID-19 and severe COVID-19 cohorts by non-parametric Kruskall-Wallis ANOVA, followed by correction for a false discovery rate (FDR) using the method of Benjamini, Krieger and Yekutieli. Features with <1% FDR were considered significant. Post-hoc bivariate comparison was done by Dunn's multiple comparison test. To correct for batch effects across CyTOF runs, signal intensities were normalized to a common reference sample by dividing the experimental sample geometric mean by the reference sample geometric mean for each feature. Normalized signal intensities

were used for downstream analysis. Cytokine data was analyzed by Kruskall-Wallis ANOVA followed by correction for a false discovery rate (FDR) using the method of Benjamini, Krieger and Yekutieli. Features with <1% FDR were considered significant. Post-hoc bivariate comparison was done by Dunn's multiple comparison test. ELISpot data was analyzed by Kruskall-Wallis ANOVA. Post-hoc bivariate comparison was done by Dunn's multiple comparison test.

Correlation between CyTOF features and soluble markers and ELISpot results was done with Spearman Rank Order Correlation.

Kruskall-Wallis and Dunn's test were run on SPSS V12 (IBM Corporation, Armonk, NY). Benjamini, Krieger and Yekutieli Analysis was done in Prism (Graphpad Software, San Diego, CA).

Results:

Mass-Cytometry Defines the Immunologic Pathways Induced by COVID-19. To define the effects of SARS-COV2 infection on the intracellular signaling environment of circulating leukocytes, we recruited a cohort of 63 subjects with COVID-19. COVID-19 severity was defined using modified WHO disease severity criteria. Critically ill patients requiring intensive care were characterized as "Severe"; patients requiring inpatient care but not intensive care were defined as "Moderate". Blood was isolated from 20 subjects with moderate illness and 43 subjects with severe illness. All samples were obtained within 3 days of hospital presentation. A cohort of healthy donors served as controls. Peripheral blood was analyzed by mass cytometry. For subsets of these patients, plasma cytokine levels and T cell interferon gamma production by ELISpot assay were assayed (Figure 1A). Demographic characteristics of all cohorts are shown in Extended Data Table 2. Subjects with severe COVID-19 had a longer length of stay

as compared to subjects with moderate COVID-19. 58% of patients with severe COVID-19 required mechanical ventilation, and within the severe COVID-19 cohort, mortality was 37%. Consistent with prior studies, clinical laboratory values demonstrated that COVID-19 was associated with leukocytosis (Figure 1B). We also identified anemia in both moderate and severe COVID-19 patients. Severe COVID-19 was associated with elevated serum creatinine, although there was no significant difference between subjects with moderate vs. severe disease. Both moderate and severe COVID-19 was associated with a coagulopathy manifest as an elevated INR; further, subjects with severe COVID-19 had increased INR as compared to moderately ill subjects (Figure 1B). Complete clinical laboratory profiles are shown in Extended Data Table 3.

We used mass-cytometry to define the immunologic features associated with COVID-19 disease. We analyzed blood using a panel of heavy-metal conjugated antibodies recognizing both cell surface antigens and intracellular signaling molecules coupled with mass cytometry (See Extended Data Table 1). Cell type was defined based on cell surface phenotype by on manual gating using canonical markers (Extended Data Figure 1). Within each population, we measured the signal intensity of 15 intracellular signaling molecules which are key mediators of T cell and monocyte response to invading pathogens. Altogether, we defined 95 cellular features that identify the dominant response of immune effector cells to COVID-19 infection (Extended Data Table 4). To understand the overall structure of the CyTOF data we performed factor reduction by Principal Component Analysis. Figure 1C shows an X-Y plot of the first two principal components, which together account for 45% of the overall variance in the dataset. Healthy subjects were tightly arrayed along a common line. In contrast, subjects with COVID-19 formed a distinct cluster with severely ill subjects having a higher variance than that of moderately ill subjects. These PCA plots demonstrate that our CyTOF features can segregate healthy donors from moderately and severely ill COVID-19 patients. To identify specific features associated with COVID-19 disease, we

used the non-parametric rank-order Kruskall-Wallis test to compare the distribution of each feature across groups (healthy controls, moderate COVID-19, severe COVID-19) and corrected for a 1% false discovery rate (FDR) using the Benjamini, Krieger and Yekutieli approach. After false-discovery correction, we identified 43 features with differential variance across condition (healthy, moderate COVID-19 and severe COVID-19, see Extended Data Table 4). To visualize the interaction between p-value, false discovery and effect size we first calculated an effect size for each feature shown in Extended Data Table 4. Effect size was estimated using a modified z-score, calculated as the difference in means between subjects with severe COVID-19 and healthy controls, divided by the standard deviation of the healthy control population. Figure 1D shows volcano plot of effect size vs. p-value, with features reaching an FDR of 1% shown in green.

To define the immunologic effects of COVID-19, on the absolute numbers of different immune effectors comprising innate and adaptive immunity, we first evaluated circulating leukocyte frequency and number. Using canonical surface markers to define leukocyte types, we measured the frequency and absolute number of circulating leukocyte cell populations. Consistent with prior studies, we found that COVID-19 was associated with an increase in neutrophil frequency, although there was a trend toward increased neutrophil numbers, this trend did not reach a statistically significant threshold. We did measure a significant decrease in frequency of both innate and adaptive leukocytes including monocytes, CD4 T cells, CD8 T cells, plasmacytoid dendritic cells (pDC) and NK cells. These differences in frequency translated to absolute leukopenia during COVID-19 for most of the cell populations measured, including monocytes, CD4 and CD8 T cells and pDC (Figure 2). We detected no differences in B-cell frequency or number.

Dysregulated Signaling Landscape Induced by Acute COVID-19. To define the effects of COVID-19 on the intracellular signaling landscape of circulating leukocytes we measured a panel of signaling phosphoproteins in neutrophils, classical monocytes, NK cells, CD4 and CD8 T cells. For each sample, leukocyte populations were manually gated based canonical markers (Extended Data Figure 1) and we measured signal intensity of phosphoproteins within each population (Extended Data Table 5). To visualize the overall structure of the data we prepared a heatmap of phosphoprotein signaling intensities in each population for all samples, then clustered based on sample and row using hierarchical clustering (Figure 3). Across samples, healthy donor clustered tightly and were distinct from subjects with COVID-19, although moderate and severe COVID-19 were intermixed (Figure 3). Hierarchical clustering across features demonstrated shared covariance of phospho- STAT1 and STAT3 (pSTAT1, pSTAT3) signals. pSTAT1 and pSTAT3 levels clustered together across cells types including neutrophils, monocytes, CD4 T cells and CD8 T cells, suggesting that STAT1 and STAT3 phosphorylation levels may distinguish the normal cellular signaling pathways operative in healthy donors versus COVID-19 induced altered signaling pathways and subjects with COVID-19 (Figure 3).

To further characterize the effect of COVID-19 on the leukocyte phosphoprotein landscape we measured the magnitude and direction of the signaling effect induced by COVID-19. Effect size was defined by a modified z-score calculated as the difference in median signaling intensity between severe COVID-19 and healthy controls, divided by the standard deviation in the control population. COVID-19 was associated with wholesale increases in signaling phosphoprotein levels. Consistent with hierarchical clustering data, we measured the largest effect sizes measured for STAT3 and STAT1 (Figure 4A). As compared to healthy donors, we found only increased levels of signaling molecule phosphorylation, and in no case was COVID-19 associated with decreased phosphoprotein signal intensity as compared to healthy donors (Figure 4A).

Within the innate immune compartment, we evaluated changes in signaling phosphoprotein levels in monocytes, NK cells and neutrophils. In monocytes, we found that as compared to healthy donors both moderate and severe COVID-19 was associated with increased phosphorylation of STAT3, CREB, MAPKAP2 and ERK; there was no difference between moderate and severe COVID-19. We saw broader but less robust activation in NK cells, including elevated levels of phosphorylated STAT1, STAT3, ERK, MAPKAP2, CREB and IκB. In neutrophils, phospho-STAT1 and phospho-ERK distinguished healthy donors for patients with COVID-19 (Figure 4B).

Among T cells, we detected broad increases in signaling protein phosphorylation in both CD4 and CD8 T cells. Notably in both populations, STAT3 phosphorylation predominated, with a >7-fold increase in phospho-STAT3 in CD4 T cells and a >3-fold increase in CD8 T cells in severe COVID-19 subjects vs. healthy donors (Figure 4C). Phospho-STAT3 levels in CD4 and CD8 T cells distinguished between healthy donors, moderate COVID-19, and severe COVID-19. STAT1, MAPKAP2, CREB and IκBα were also increased in severe COVID-19 in both T cell populations. In both CD4 and CD8 T cells, MAPKAP2 and ITK/BTK phosphoprotein levels were increased in moderate vs. healthy donors. In contrast with the innate immune cell populations, we did not detect significant levels of ERK phosphorylation in CD4 or CD8 T cells (Figure 4C).

During COVID-19 Inflammatory Cytokines are associated with STAT3 and ERK phosphorylation in Circulating Leukocytes. To define the interactions between the leukocyte phosphoproteome and the systemic inflammatory response during COVID-19, we measured plasma levels of 36 cytokines and chemokines in a subset of the subjects using a multiplexed assay (see Extended Data Table 5).

Hierarchical clustering identified 4 cytokine clusters, with inflammatory mediators including IL-6, IL-8, CXCL-10 and HGF clustered together (Extended data Figure 2). Consistent with prior studies, we found that IL-6, IL-8, IL-1RA, CXCL-10 distinguished healthy controls from both moderate and severe COVID-19 cases (Figure 5A). In addition, HGF and MCP-1 distinguished moderate from severe COVID-19 (Figure 5A).

To understand the pathways driving cellular activation in neutrophils, monocytes and NK cells, we evaluated the relationship between phosphoprotein levels and circulating cytokine levels by measuring the correlation between phosphoprotein levels and cytokine levels across all samples (healthy, moderate COVID-19 and Severe COVID-19). Figure 5B shows a heatmap of Spearman correlation coefficients and 5C shows scatter plots of a subset of highly correlated features. In monocytes and NK cells, phospho-STAT3 levels were strongly correlated with circulating levels of IL-6 and CXCL10. In neutrophils phospho-STAT1 was highly correlated with IL-6 and CXCL10 as were levels of phospho-STAT1 in neutrophils. In contrast, monocyte phospho-ERK levels were most correlated with plasma levels of IL-8 (Figure 5A/B).

We applied a similar approach to define the signaling pathways activated in circulating CD4 and CD8 T cells. We again sought to correlate protein phosphorylation with circulating cytokine levels. In both CD4 and CD8 T cells, STAT1 and STAT3 phosphorylation were strongly correlated with IL-6, CXCL10, IL-8 and IL-1RA levels (Figure 6A/B). Consistent with the canonical signaling downstream of the IL-6 receptor[28, 29, 30], CD4 T cell pSTAT3 was most highly correlated with circulating IL-6 levels, with a Spearman R of 0.85. This suggest that circulating IL-6 drives CD4 T cell STAT3 activation during acute COVID-19.

Signaling Phosphoprotein Levels Correlate with Immune Cell Functional Metrics. Severe COVID-19 is associated with a dysregulation of the myeloid cell compartment characterized by increased numbers of immature neutrophils in circulation, a shift to HLA-DR-lo monocytes and defects in the function of mature neutrophils in the circulation. Prior work has characterized significant heterogeneity in the circulating neutrophil compartment induced by COVID-19, including accumulation of neutrophils expressing decreased levels of HLA-DR, CD15, CD11b. Consistent with this, we detected decreased mean surface expression of HLA-DR and CD15 on the neutrophils during both moderate and severe COVID-19 as compared to healthy donors. CD11b significantly decreased in severe COVID-19 as compared to both healthy donors and subjects with moderate COVID-19 disease. We also evaluated the relationship between changes in phosphoprotein levels and surface marker expression. In neutrophils, we found that surface CD11b levels were negatively correlated with intracellular phospho-ERK (pERK) levels, with lower mean levels of CD11b in samples with higher pERK levels. Surface expression of CD15 on neutrophils was more tightly (and negatively) correlated with phospho-STAT1 levels (Figure 6B). Similarly, we found lower levels of CD11b, HLA-DR, CD14 and CD33 on the monocyte surface (Figure 6C). In monocytes, we again measured a negative correlation between increased signaling phosphoprotein levels and surface marker expression. In monocytes, CD11b levels were negatively correlated with phospho-STAT3 levels and HLA-DR levels correlated with phospho-CREB levels (Figure 6D).

We have previously shown that critical illness including COVID-19 is associated with adaptive immune dysfunction as measured by defects in T cell IFN-γ production in response to *ex vivo* T cell receptor stimulation[22]. Consistent with these data, we found that COVID-19 was associated with attenuated production of IFN- γ after stimulation of peripheral blood mononuclear cells with agonistic antibodies against CD3/CD28, suggesting a defect in T cell function during COVID-19 as compared to healthy controls (Figure 6E). We then assessed the relationship between phosphoprotein levels and T cell

function. We found that increased pSTAT3 levels in both CD4 and CD8 T cells was associated with decreased production of IFN-γ in response to CD3/CD28 stimulation, suggesting increased STAT3 activation as a mechanism for defects in T cell function during COVID-19.

Discussion:

We deployed a systems biology approach centered on a mass-cytometry phosphoproteome assay combined with multiplexed measurement of circulating cytokine levels and ex-vivo stimulated T cell function by ELISpot to define the effect of COVID-19 on the intracellular signaling landscape of circulating leukocytes during acute COVID-19. We find that COVID-19 is associated with a wholesale increase in signaling protein phosphorylation in both myeloid and lymphoid cell populations across multiple signaling pathways. In all cell populations there was a strong, *positive* correlation between an activated phosphoproteome signature and circulating inflammatory cytokine levels. In particular, STAT3 activation was tightly correlated with plasma IL-6 levels. In myeloid cells signaling protein phosphorylation levels were *negatively* correlated with surface markers of activation and maturation. Similarly, in T cells, *increased* STAT3 phosphorylation was specifically associated with *defects* in IFN-γ production. These data reconcile the coincident inflammatory cytokinemia and functional immunosuppression induced by COVID-19 and suggest modulation of STAT3 as a potential therapeutic avenue to restore T cell function during severe COVID-19.

Consistent with past studies[16, 17, 18], we found that COVID-19 was associated with an increase in neutrophil frequency and a concomitant decrease in other circulating leukocyte populations including monocytes, basophils and both CD4 and CD8 T cells. The increased neutrophil frequency was associated with a decreased expression of surface markers of maturation including CD11b, HLA-DR and CD15. COVID-19 is associated with accumulation of peripherally circulating immature low-density neutrophils (LDN)[14], previously characterized to have low-to-intermediate surface expression of CD11b[13] and HLA-DR[13, 14, 15]. Similarly, CD15 is a marker of neutrophil antimicrobial function, with decreased CD15 expression being associated with high TB microbial burden and treatment failure[31]. We also found

decreased expression of monocyte maturation markers including CD33, CD14 and HLA-DR. This observation is consistent with studies showing that IL-6 is a suppressive cytokine to monocyte CD33 and CD14 levels[32]. This shift in surface marker phenotype likely reflects emergency hematopoiesis[33] with mobilization of immature neutrophils from the bone-marrow driven both by margination of mature neutrophils to the lungs and mobilization of immature cells by inflammatory cytokines including IL-6 and IL-8[34].

To our knowledge this is the first description of the signaling phosphoproteome in peripheral blood leukocytes during acute infection with SARS-COV2. COVID-19 was associated with an overall increase in signaling protein phosphorylation, and in no case was there a decreased protein phosphorylation in COVID-19 vs. controls. We found that circulating leukocyte phosphoprotein signature alone can distinguish subjects with COVID-19 from healthy donor controls. In all cell populations, STAT3 was the predominant signaling pathway activated during COVID-19. STAT3 is the predominant downstream target of the IL-6 receptor [28, 30]. COVID-19 induces high levels of circulating IL-6, and we found that phospho-STAT3 levels were tightly correlated with plasma IL-6 levels. Although we detected upregulation of multiple signaling pathways, the specific increase in STAT3 phosphorylation during COVID-19 was striking.

STAT3 is an evolutionarily primordial signaling molecule with pleiotropic effects in both immune and non-immune tissues including mediating lymphocyte differentiation and function, myeloid cell activation, emergency hematopoiesis and the hepatic acute phase response[35, 36]. We found near universal increases in STAT3 phosphorylation during both moderate and severe COVID-19, likely reflecting persistent STAT3 activity in both monocytes and lymphocytes. Although STAT3 is canonically associated with immune cell activation and transcription of pro-inflammatory genes, exaggerated STAT3

activation can results in immunosuppression[36, 37, 38]. Genetic STAT3 gain of function (GOF) mutations result in persistent, chronic STAT3 activity, and phenocopies the changes in peripheral leukocyte populations seen in severe COVID-19, with decreased circulating levels of pDC, NK cells and Th17 lymphocytes[39, 40]. These patients are also at higher risk of disseminated mycobacterial infection[39, 41], concerning for defects in antigen presenting cell function. In part the immunosuppressive effects of STAT3 reflects fine-tuning of the STAT3 transcriptional response by SOCS3, which suppresses STAT3 immunosuppressive activity[42]. In the absence of SOCS3 activity, STAT3 activation induced by IL-6 can lead to decreased expression of MHC-II molecules and co-stimulatory molecules on the surface of antigen presenting cells. In-vitro data support this observation, with STAT3 repressing transcription of pro-inflammatory genes after persistent LPS stimulation. Transcriptome studies have reported decreased levels of SOCS-3 in myeloid cells during COVID-19[43], which could lead to an immunosuppressive response to IL-6-mediated STAT3 activation during COVID-19. This hypothesis is consistent with studies demonstrating defects in dendritic cell response during COVID-19[23, 43], the depressed monocyte surface expression of HLA-DR and CD86 reported here, and our previously published data demonstrating that COVID-19 is associated with decreased LPS-induced TNF-alpha production by peripheral blood mononuclear cells.

STAT3 has also been also been shown to inhibit the Type-I IFN antiviral response. COVID-19 is associated with increased circulating levels of IFN-alpha[26], and our analysis did measure a 2-fold increase in IFN-alpha in severe COVID vs. healthy donors (although these data did not meet the threshold for a 1% FDR, see Extended Data Table 5). Transcriptomic studies detected expression of Interferon-stimulated genes (ISG) in mild and moderate COVID-19, but an impaired Type-I interferon response in severe COVID-19[44, 45]. Others reproduced these results, finding that severe influenza was associated with upregulation of ISG which was not seen in severely ill COVID-19 patient[26]. STAT3-mediated inhibition of the IFN response

is independent of STAT3 transcriptional activity and is mediated through negative regulation of the cytosolic dsRNA receptor MDA5[44]. MDA5 serves as a pattern recognition receptor for SARS-CoV2 underlying the IFN response during COVID-19[46], and the decreased ISG expression during COVID-19 may result from increased STAT3 mediated inhibition of MDA5 activity.

We acknowledge several limitations in our study. Foremost, our study design provides limited clinical information for our cohort of COVID-19 subjects, and we have not associated our findings with clinical outcomes from COVID-19. We have segregated our patients into “moderate” and “severe” COVID-19 disease, and we do report clinical outcomes including ICU admission, ventilator days and hospital length of stay are segregate based on disease severity, and we report differences in signaling phosphoproteome between our cohorts, but our limited sample size and limited clinical data constrains our ability to do a controlled analysis of the relationship between specific phosphoproteome features and clinical outcome. We predict that phospho-STAT3 levels on hospital admission may have prognostic significance, but this hypothesis will require further investigation. Our data analysis approach also has limitations. We have analyzed our CyTOF data by manual gating of canonical markers. We have only compared signaling protein phosphorylation across a limited set of major circulating populations. We recognize that by aggregating together leukocyte subpopulations, we may obscure differences in phosphoprotome activation in leukocyte subpopulations. The data utilized for this study will be made available in publicly accessible database, and we encourage collaborating investigators to undertake further analysis to elucidate these differences.

Given these limitations, these data demonstrate that COVID-19 causes an acute dysregulation of the signaling landscape of circulating leukocytes, defined primarily by exaggerated phosphorylation of STAT3. In both myeloid and lymphoid cell populations, pSTAT3 levels are correlated with evidence of

functional immunosuppression, suggesting STAT3 blockade as a potential therapeutic pathway to restore immunocompetence during severe COVID-19. Prior reports have advocated STAT3 inhibition to restrain inflammation-mediated tissue damage[10, 12]. These reports extend from a hypothesized role for STAT3 in the immunopathology of COVID-19 through the IL-6 amplifier pathway, whereby STAT3 and NFκB synergize to drive inflammatory gene transcription locally in non-immune tissue, driving inflammation-mediated tissue injury[47]. We propose that dysregulated STAT3 activation reconciles local inflammation-mediated tissue damage and systemic functional immunosuppression, and suggests that pharmacologic inhibition of STAT3 may simultaneously restrain local inflammation-mediated tissue damage while restoring systemic antiviral immune function.

Acknowledgements:

This work is supported NIH grants R35GM133756, UL1TR002345, R35GM126928 and the Rubin Family Research Fund. This work was supported by the Washington University Institute for Clinical and Translational Sciences WU350 Study. We would also like to acknowledge our colleagues working at Barnes Jewish Hospital and the Missouri Baptist Medical Center for the excellent care they provided to the patients in this study.

References:

1. WHO. WHO Coronavirus Disease (COVID-19) Dashboard. [cited February 10,2021]Available from: https://covid19.who.int/

2. CDC COVID Data Tracker. [cited Feburary 10, 2021]Available from: https://covid.cdc.gov/covid-data-tracker/#datatracker-home

3. Yang, X. *et al.* Clinical course and outcomes of critically ill patients with SARS-CoV-2 pneumonia in Wuhan, China: a single-centered, retrospective, observational study. *The Lancet. Respiratory medicine* **8**, 475-481 (2020).

4. Wang, D. *et al.* Clinical Characteristics of 138 Hospitalized Patients With 2019 Novel Coronavirus-Infected Pneumonia in Wuhan, China. *JAMA : the journal of the American Medical Association* **323**, 1061-1069 (2020).

5. Wu, Z. & McGoogan, J.M. Characteristics of and Important Lessons From the Coronavirus Disease 2019 (COVID-19) Outbreak in China: Summary of a Report of 72 314 Cases From the Chinese Center for Disease Control and Prevention. *JAMA : the journal of the American Medical Association* **323**, 1239-1242 (2020).

6. Guan, W.J. *et al.* Clinical Characteristics of Coronavirus Disease 2019 in China. *The New England journal of medicine* **382**, 1708-1720 (2020).

7. Vahidy, F.S. *et al.* Characteristics and Outcomes of COVID-19 Patients During Initial Peak and Resurgence in the Houston Metropolitan Area. *JAMA : the journal of the American Medical Association* **324**, 998-1000 (2020).

8. Hotchkiss, R.S. *et al.* Sepsis and septic shock. *Nature reviews. Disease primers* **2**, 16045 (2016).

9. Mehta, P. *et al.* COVID-19: consider cytokine storm syndromes and immunosuppression. *Lancet* **395**, 1033-1034 (2020).

10. Hojyo, S. *et al.* How COVID-19 induces cytokine storm with high mortality. *Inflammation and regeneration* **40**, 37 (2020).

11. Chen, G. *et al.* Clinical and immunological features of severe and moderate coronavirus disease 2019. *The Journal of clinical investigation* **130**, 2620-2629 (2020).

12. Hirano, T. & Murakami, M. COVID-19: A New Virus, but a Familiar Receptor and Cytokine Release Syndrome. *Immunity* **52**, 731-733 (2020).

13. Carissimo, G. *et al.* Whole blood immunophenotyping uncovers immature neutrophil-to-VD2 T-cell ratio as an early marker for severe COVID-19. *Nature communications* **11**, 5243 (2020).

14. Schulte-Schrepping, J. *et al.* Severe COVID-19 Is Marked by a Dysregulated Myeloid Cell Compartment. *Cell* **182**, 1419-1440.e1423 (2020).

15. Silvin, A. *et al.* Elevated Calprotectin and Abnormal Myeloid Cell Subsets Discriminate Severe from Mild COVID-19. *Cell* **182**, 1401-1418.e1418 (2020).

16. Mathew, D. *et al.* Deep immune profiling of COVID-19 patients reveals distinct immunotypes with therapeutic implications. *Science* **369** (2020).

17. Laing, A.G. *et al.* A dynamic COVID-19 immune signature includes associations with poor prognosis. *Nature medicine* **26**, 1623-1635 (2020).

18. Kuri-Cervantes, L. *et al.* Comprehensive mapping of immune perturbations associated with severe COVID-19. *Science immunology* **5** (2020).

19. Zhu, L. *et al.* Single-Cell Sequencing of Peripheral Mononuclear Cells Reveals Distinct Immune Response Landscapes of COVID-19 and Influenza Patients. *Immunity* **53**, 685-696.e683 (2020).

20. Tian, W. *et al.* Immune suppression in the early stage of COVID-19 disease. *Nature communications* **11**, 5859 (2020).

21. Ritchie, A.I. & Singanayagam, A. Immunosuppression for hyperinflammation in COVID-19: a double-edged sword? *Lancet* **395**, 1111 (2020).

22. Remy, K.E. *et al.* Severe immunosuppression and not a cytokine storm characterizes COVID-19 infections. *JCI insight* **5** (2020).

23. Zhou, R. *et al.* Acute SARS-CoV-2 Infection Impairs Dendritic Cell and T Cell Responses. *Immunity* **53**, 864-877.e865 (2020).

24. Mudd, P.A. *et al.* Distinct inflammatory profiles distinguish COVID-19 from influenza with limited contributions from cytokine storm. *Science advances* (2020).

25. De Biasi, S. *et al.* Marked T cell activation, senescence, exhaustion and skewing towards TH17 in patients with COVID-19 pneumonia. *Nature communications* **11**, 3434 (2020).

26. Lee, J.S. *et al.* Immunophenotyping of COVID-19 and influenza highlights the role of type I interferons in development of severe COVID-19. *Science immunology* **5** (2020).

27. Wilk, A.J. *et al.* A single-cell atlas of the peripheral immune response in patients with severe COVID-19. *Nature medicine* **26**, 1070-1076 (2020).

28. Wegenka, U.M. *et al.* The interleukin-6-activated acute-phase response factor is antigenically and functionally related to members of the signal transducer and activator of transcription (STAT) family. *Molecular and cellular biology* **14**, 3186-3196 (1994).

29. Aaronson, D.S. & Horvath, C.M. A road map for those who don't know JAK-STAT. *Science* **296**, 1653-1655 (2002).

30. Akira, S. *et al.* Molecular cloning of APRF, a novel IFN-stimulated gene factor 3 p91-related transcription factor involved in the gp130-mediated signaling pathway. *Cell* **77**, 63-71 (1994).

31. Ndlovu, L.N. *et al.* Increased Neutrophil Count and Decreased Neutrophil CD15 Expression Correlate With TB Disease Severity and Treatment Response Irrespective of HIV Co-infection. *Frontiers in immunology* **11**, 1872 (2020).

32. Roussel, M. *et al.* Mass cytometry deep phenotyping of human mononuclear phagocytes and myeloid-derived suppressor cells from human blood and bone marrow. *Journal of leukocyte biology* **102**, 437-447 (2017).

33. Loftus, T.J., Mohr, A.M. & Moldawer, L.L. Dysregulated myelopoiesis and hematopoietic function following acute physiologic insult. *Current opinion in hematology* **25**, 37-43 (2018).

34. Takizawa, H., Boettcher, S. & Manz, M.G. Demand-adapted regulation of early hematopoiesis in infection and inflammation. *Blood* **119**, 2991-3002 (2012).

35. Levy, D.E. & Lee, C.K. What does Stat3 do? *The Journal of clinical investigation* **109**, 1143-1148 (2002).

36. Hillmer, E.J., Zhang, H., Li, H.S. & Watowich, S.S. STAT3 signaling in immunity. *Cytokine & growth factor reviews* **31**, 1-15 (2016).

37. Wang, H. *et al.* STAT3 Regulates the Type I IFN-Mediated Antiviral Response by Interfering with the Nuclear Entry of STAT1. *International journal of molecular sciences* **20** (2019).

38. Chang, Z., Wang, Y., Zhou, X. & Long, J.E. STAT3 roles in viral infection: antiviral or proviral? *Future virology* **13**, 557-574 (2018).

39. Haapaniemi, E.M. *et al.* Autoimmunity, hypogammaglobulinemia, lymphoproliferation, and mycobacterial disease in patients with activating mutations in STAT3. *Blood* **125**, 639-648 (2015).

40. Flanagan, S.E. *et al.* Activating germline mutations in STAT3 cause early-onset multi-organ autoimmune disease. *Nature genetics* **46**, 812-814 (2014).

41. Wang, J. *et al.* Leptin correlates with monocytes activation and severe condition in COVID-19 patients. *Journal of leukocyte biology* (2021).

42. Tsai, M.H., Pai, L.M. & Lee, C.K. Fine-Tuning of Type I Interferon Response by STAT3. *Frontiers in immunology* **10**, 1448 (2019).

43. Parackova, Z. *et al.* Disharmonic Inflammatory Signatures in COVID-19: Augmented Neutrophils' but Impaired Monocytes' and Dendritic Cells' Responsiveness. *Cells* **9** (2020).

44. Wang, W.B., Levy, D.E. & Lee, C.K. STAT3 negatively regulates type I IFN-mediated antiviral response. *Journal of immunology (Baltimore, Md. : 1950)* **187**, 2578-2585 (2011).

45. Hadjadj, J. *et al.* Impaired type I interferon activity and inflammatory responses in severe COVID-19 patients. *Science* **369**, 718-724 (2020).

46. Yin, X. *et al.* MDA5 Governs the Innate Immune Response to SARS-CoV-2 in Lung Epithelial Cells. *Cell reports* **34**, 108628 (2021).

47. Ogura, H. *et al.* Interleukin-17 promotes autoimmunity by triggering a positive-feedback loop via interleukin-6 induction. *Immunity* **29**, 628-636 (2008).

Figure 1

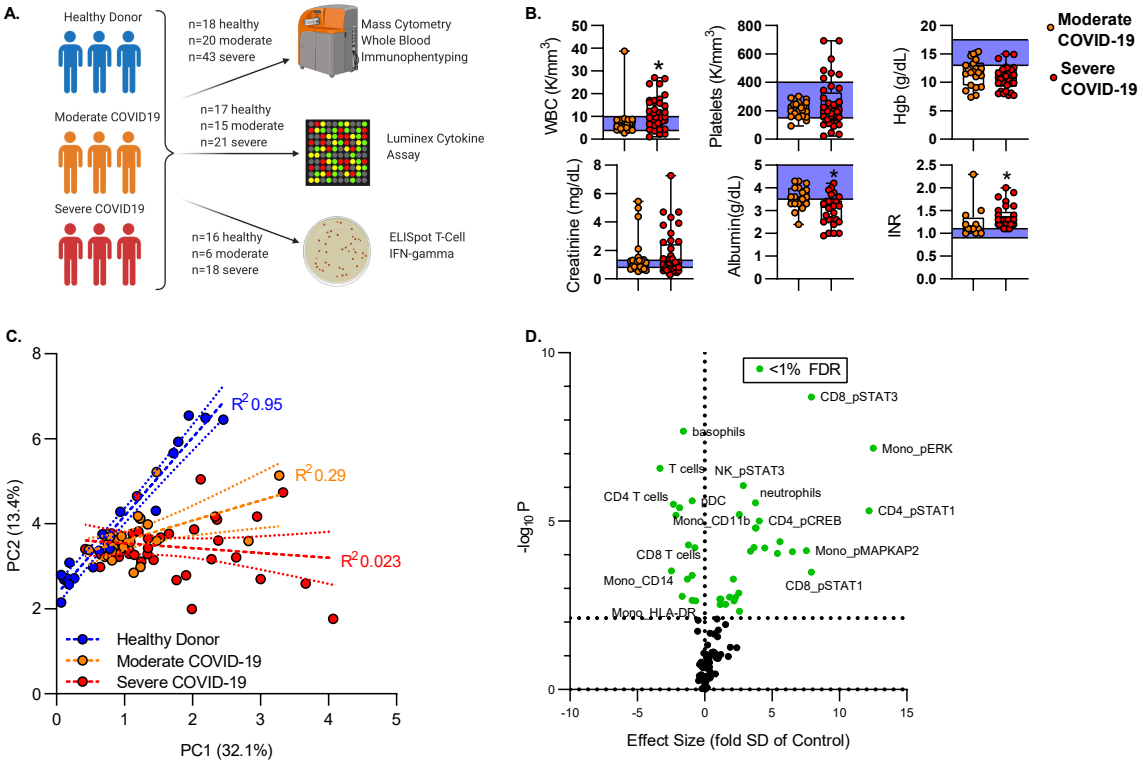

Figure 1. Mass Cytometry to Define the Molecular Mechanisms of COVID19. A) Study overview. Peripheral blood was isolated from healthy donors or patients with COVID19. All subjects were recruited within 72 hours of hospital admission. Moderate severity was defined as acute illness requiring hospitalization; severe illness as subjects with critical illness requiring ICU care. Whole blood was fixed for stored for batch CyTOF analysis. Plasma was stored for soluble marker analysis. Peripheral blood mononuclear cells were isolated by density gradient centrifugation for T cell function assay by ELISpot. **B)** Clinical laboratory values of patients with COVID19. Box plots represent 25-75th percentile with line defining group median, with all data-points overlying. Error bars extend from minimum to maximum values. Shaded area represents the normal value reference range. *p<0.05, **p<0.01, ***p<0.001, ****p<0.0001 vs moderate COVID19 by Mann-Whitney U test. **C)** Principal Component Analysis of 95 cellular featured define by CyTOF. Dashed lines represent linear regression line of the first two principal components for each cohort (healthy, moderate COVID, severe COVID); dotted lines show the 95% confidence intervals. **D)** Volcano plot of features defined by CyTOF. Effect size defined as difference of means of severe COVID vs. healthy, divided by standard deviation of healthy. P-value was measured by nonparametric (Kruskal-Wallis) ANOVA across cohorts. Significance defined as false discovery rate (FDR)< 1% by Benjamini, Krieger and Yekutieli FDR<1%=p<0.0058 (dotted line). Features that vary significantly across groups shown in green.

Figure 2

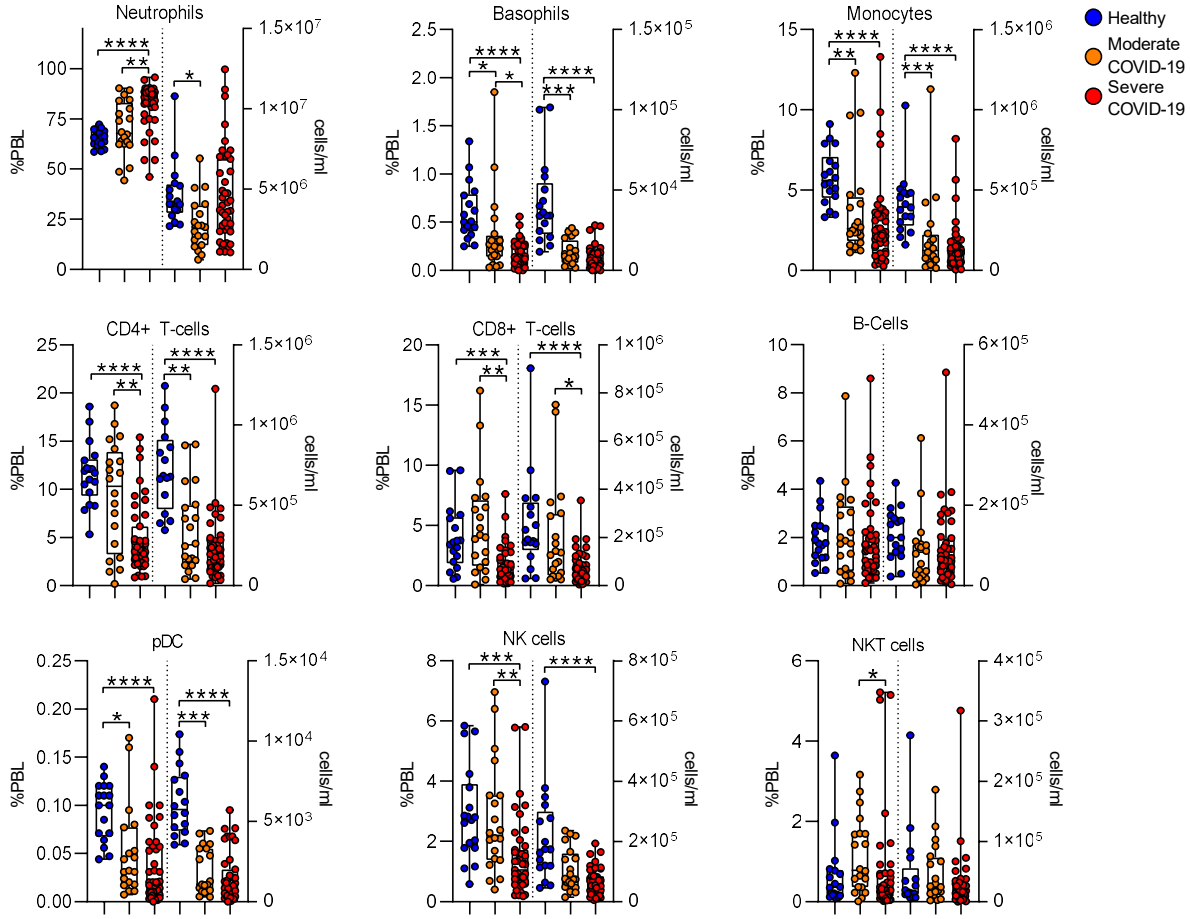

Figure 2. Effect of COVID-19 on Circulating Leukocyte Populations. Leukocyte populations were manually gated based on canonical surface marker expression. The frequency of within CD45+ peripheral blood leukocytes (%PBL) and the absolute concentration of cells (cells/ml) were calculated. Box plots represent 25-75th percentile with line defining group median, with all data-points overlying. Error bars extend from minimum to maximum values.*p<0.05, **p<0.01, ***p<0.001, ****p<0.0001 by Dunn's multiple comparisons test after nonparametric (Kruskal-Wallis) ANOVA with correction FDR<1% (Benjamini, Krieger and Yekutieli).

Figure 3

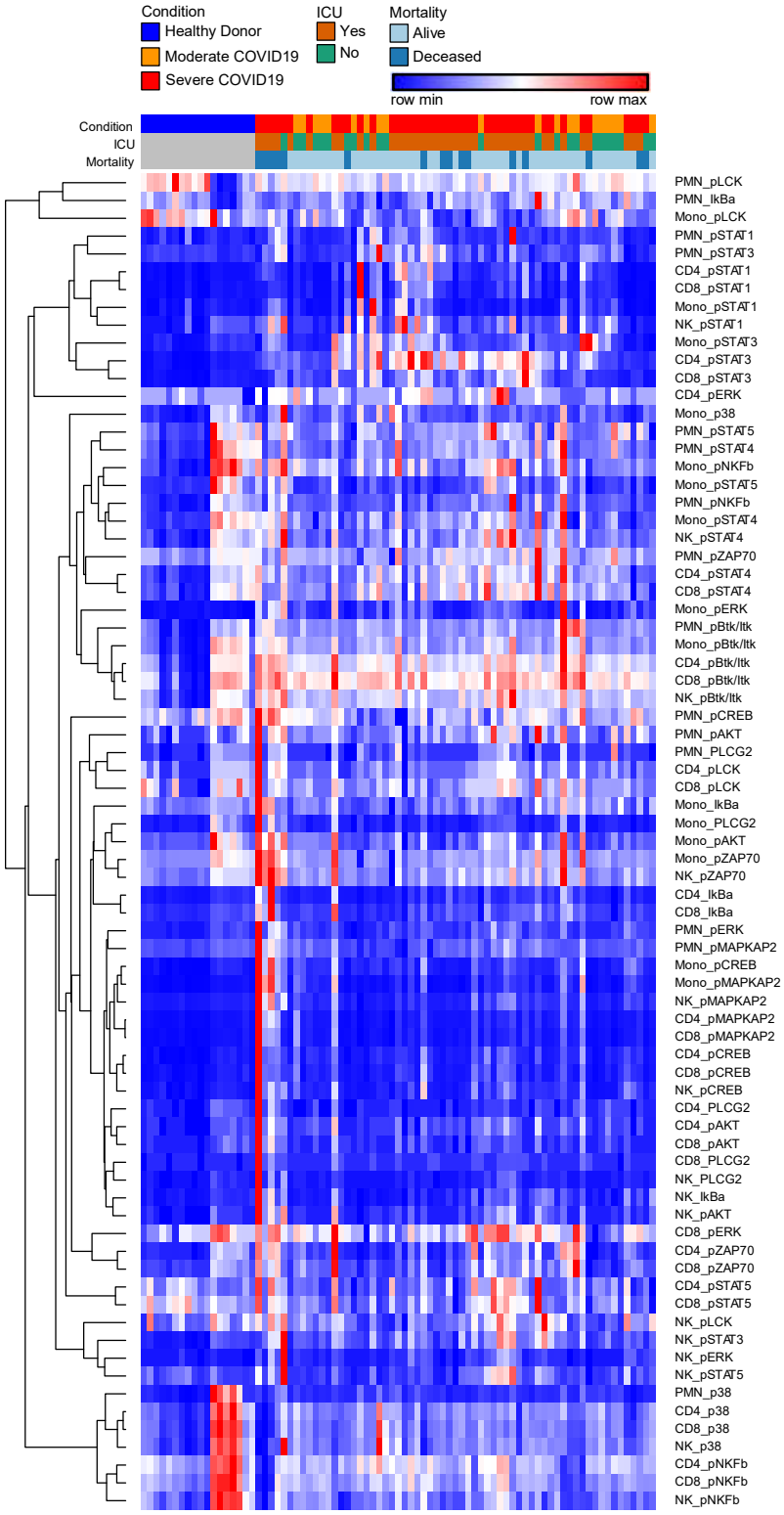

Figure 3. Heatmap of Hierarchically Clustered Signaling Phosphoprotein Levels. Columns are individual samples and rows are cellular phosphoprotein features as labelled. Values are hierarchically clustered on columns and rows. Color values are normalized to row min-max.

Figure 4

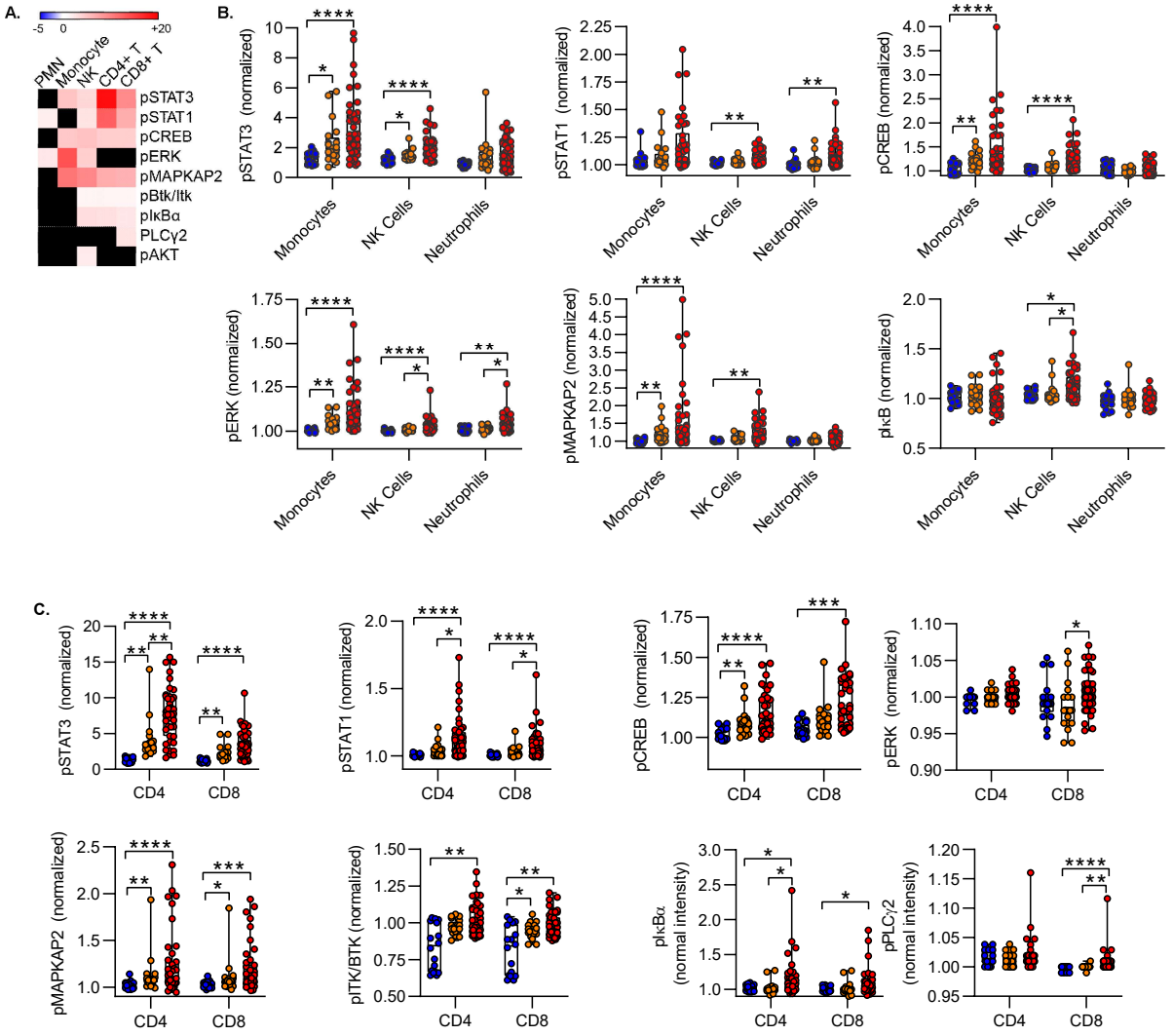

Figure 4. Effect of COVID-19 on Circulating Leukocyte Phosphoproteome. A) Heat map of effect size of severe COVID-19 vs. healthy controls for statistically significant signaling features distinguishing COVID-19 from healthy control. Effect size defined as difference of means of severe COVID vs. healthy, divided by standard deviation of healthy. **B-C)** Phosphoprotein levels in innate **(B)** and adaptive **(C)** leukocytes. To correct for CyTOF batch effects, all signal intensities are normalized to a common reference control and shown as fold-change of the reference control. Box plots represent 25-75th percentile with line defining group median, with all data-points overlying. Error bars extend from minimum to maximum values. .*p<0.05, **p<0.01, ***p<0.001, ****p<0.0001 by Dunn's multiple comparisons test after nonparametric (Kruskal-Wallis) ANOVA with correction FDR<1% (Benjamini, Krieger and Yekutieli).

Figure 5

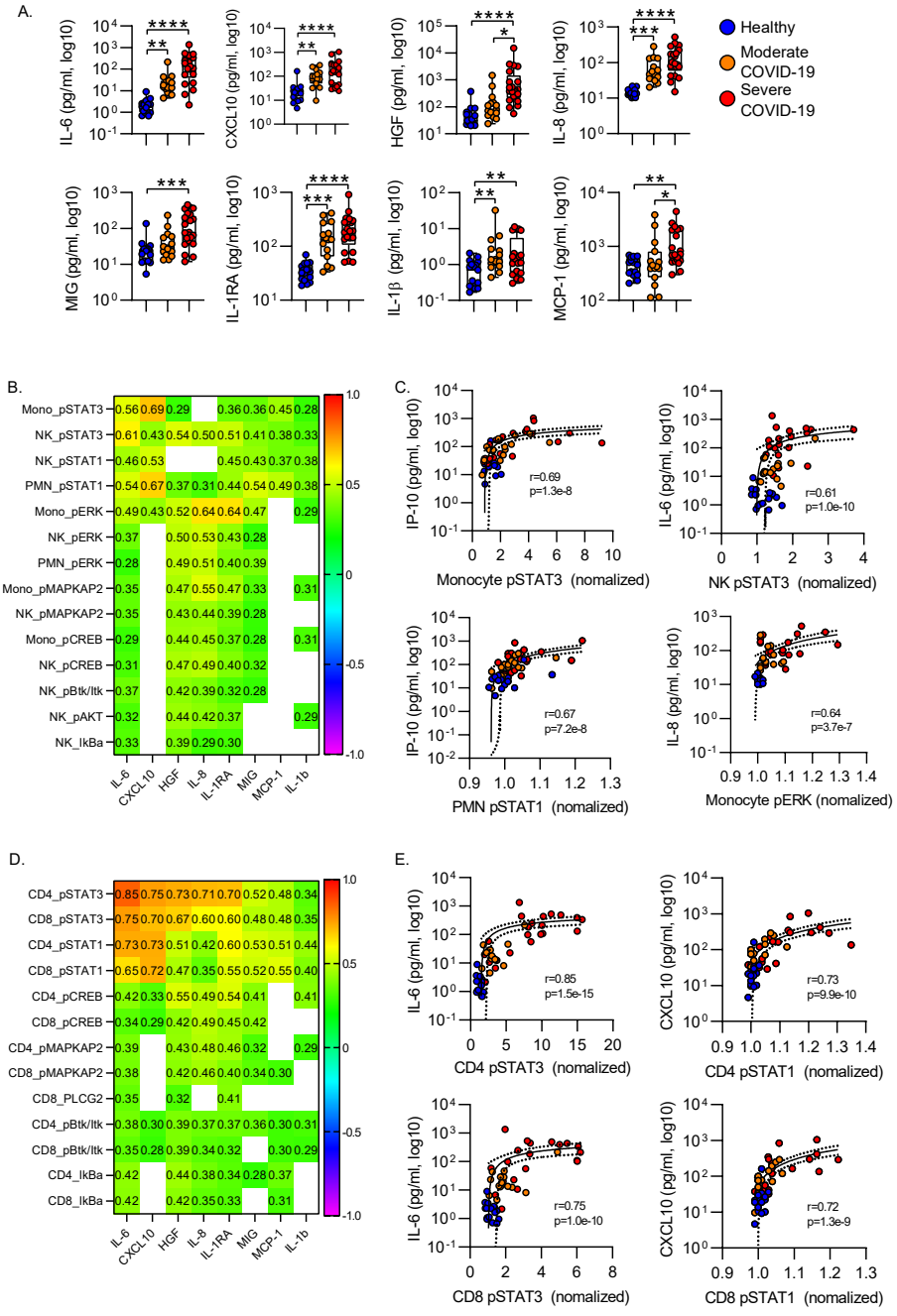

Figure 5. Correlation of Inflammatory Cytokines with Leukocyte Phosphoproteome. A) Plasma cytokines were measured in a multiplex cytokine assay. *p<0.05, **p<0.01, ***p<0.001, ****p<0.0001 by Dunn's multiple comparisons test after nonparametric (Kruskal-Wallis) ANOVA with correction for FDR<1% (Benjamini, Krieger and Yekutieli). Box plots represent 25-75th percentile with line defining group median, with all data-points overlying. Error bars extend from minimum to maximum values. **B)** Heatmap of Spearman correlation between phosphoprotein signal intensity and plasma cytokine levels. Cell values show Spearman R for correlation with p<0.05. **C)** Correlation between cellular phosphoprotein levels and plasma cytokine for highly correlated featured. Plots display correlation results from Spearman correlation test and semilog regression curve (solid line) with 95% confidence intervals (dotted lines).

Figure 6

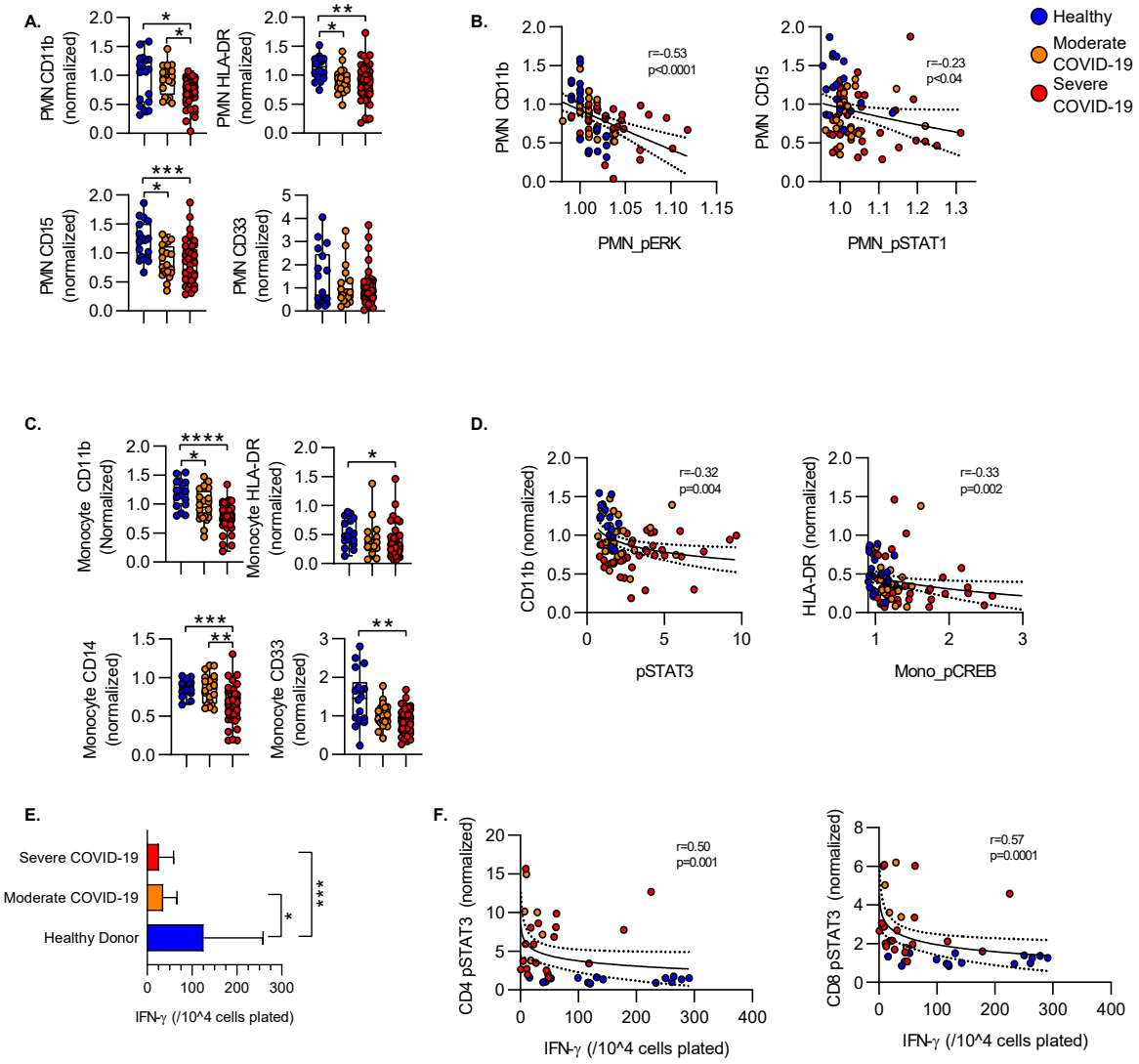

Figure 6. Activation Markers and Cytokine Production. A) Levels of surface marker expression on circulating neutrophils. **B)** Correlation between neutrophil surface marker expression level and intracellular phosphoprotein levels. **C)** Levels of surface marker expression on circulating neutrophils. **D)** Correlation between neutrophil surface marker expression level and intracellular phosphoprotein levels. **E)** IFN-γ production measured by ELISpot. PBMC were stimulated with CD3/CD28 antibodies and the number of IFN-γ producing cells enumerated. Bars show median spot number/10^4 cells +/- interquartile range. **F)** Correlation between ELIspot IFN-gamma production and intracellular phosphoprotein expression. Correlation plots display results from Spearman correlation test and semilog regression curve (solid line) with 95% confidence intervals (dotted lines).). Box plots represent 25-75th percentile with line defining group median, with all data-points overlying. Error bars extend from minimum to maximum values.*p<0.05, **p<0.01, ***p<0.001, ****p<0.0001 by Dunn's multiple comparisons test after nonparametric (Kruskal-Wallis) ANOVA with correction for FDR<1% (Benjamini, Krieger and Yekutieli).

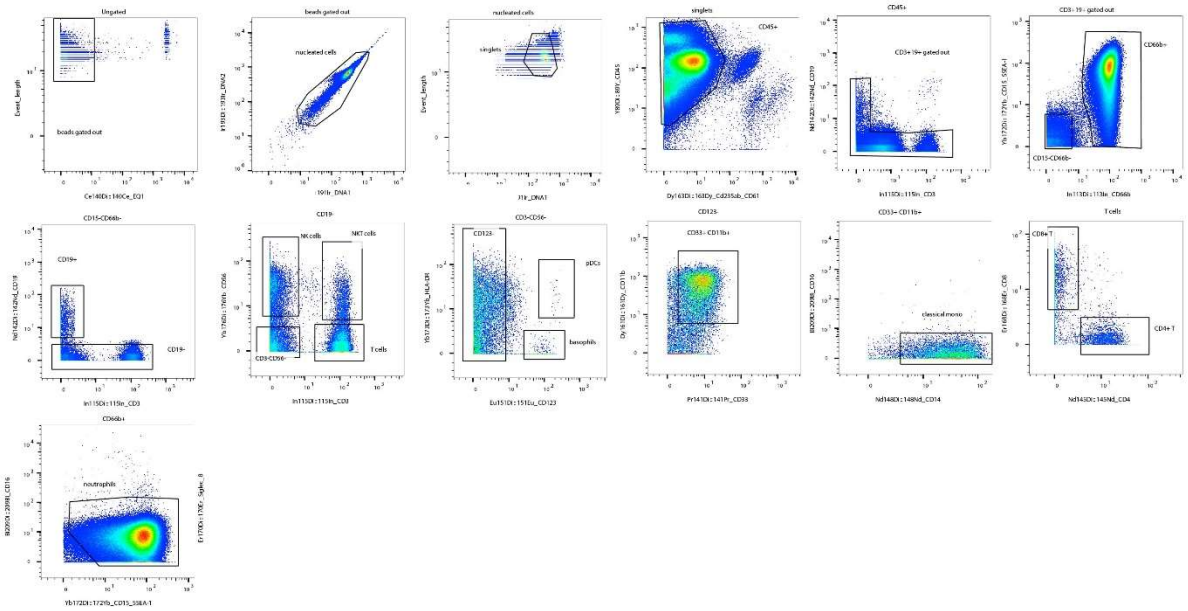

Extended Data Figure 1. Gating Strategy for Mass Cytometry.

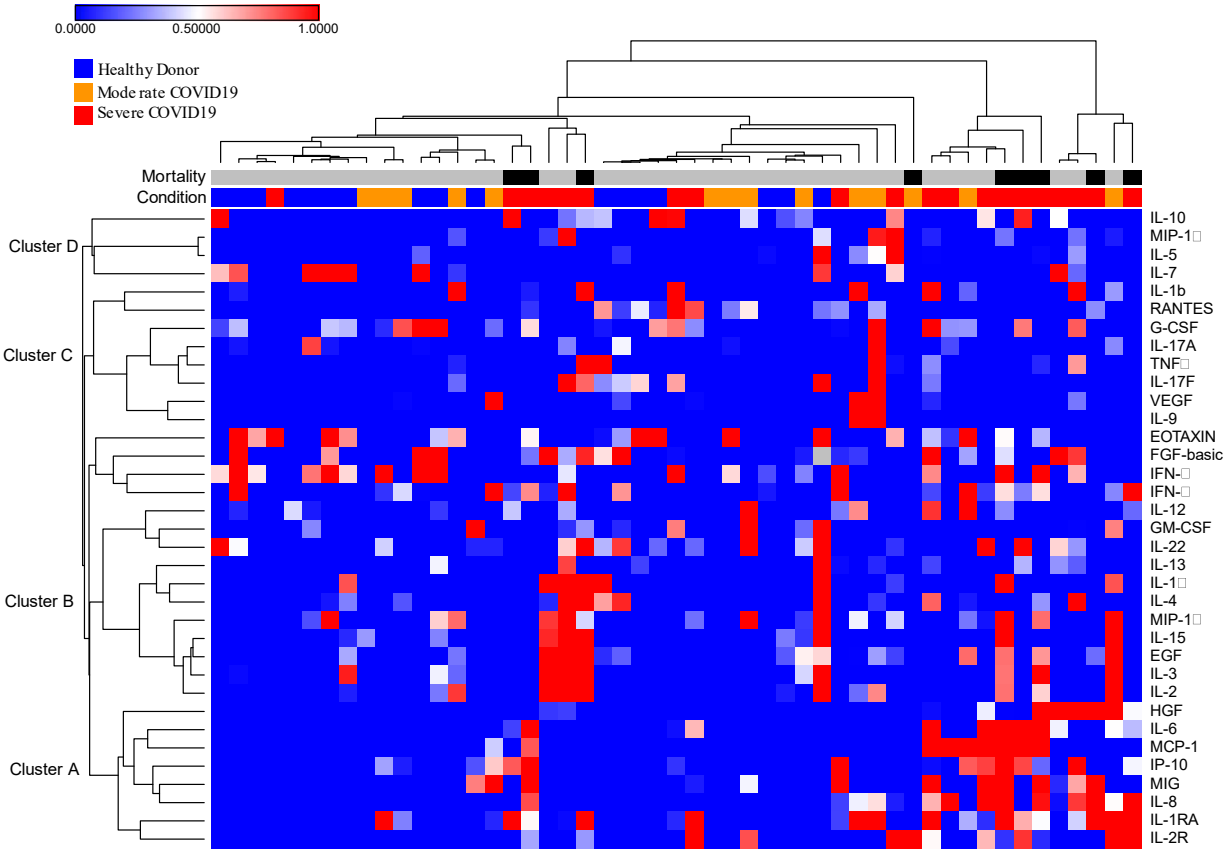

Extended Data Figure 2. Heatmap of Cytokine data. Columns are individual samples and rows are cellular phosphoprotein features as labelled. Values are hierarchically clustered on columns and rows. Color values are normalized to row min-max.

Label	Target	Clone	Manufacturer	Titer
Surface Staining Panel				
089Y	CD45	HI30	Fluidigm	1x
113In	CD66b	B1.1*	BD Biosciences	0.312 µg/ml
115In	CD3	UCHT1	Biolegend	0.544 µg/ml
141Pr	CD33	WM53*	Biolegend	0.312 µg/ml
142Nd	CD19	HIB19	Fluidigm	0.062x
143Nd	CD127	A019D5	Fluidigm	1x
145Nd	CD4	RPA-T4	Fluidigm	0.125x
147Sm	CD11c	Bu15	Fluidigm	0.125x
148Nd	CD14	RMO52	Fluidigm	0.016x
149Sm	CD45RO	UCHL1	Fluidigm	0.25x
151Eu	CD123	6H6	Fluidigm	0.109x
155Gd	CD27	L128	Fluidigm	0.062x
160Gd	CD69	FN50	BioLegend	0.625x
161Dy	CD11b (Mac-1)	ICRF44*	Biolegend	0.312 µg/ml
163Dy	CD235ab	HIR2	Fluidigm	0.109x
163Dy	CD61	VI-PL2*	Biolegend	0.033 µg/ml
168Er	CD8	SK1	Fluidigm	0.031x
169Tm	CD25	2A3	Fluidigm	0.062x
170Er	Siglec 8	7C9*	Biolegend	2.5 µg/ml
172Yb	CD15 (SSEA-1)	W6D3	Fluidigm	0.125x
173Yb	HLA-DR	L243	Fluidigm	0.031x
175Lu	PD-1	EH12.2H7	Fluidigm	0.062x
176Yb	CD56	NCAM16.2	Fluidigm	0.109x
209Bi	CD16	3G8	Fluidigm	0.062x
Intracellular Staining Panel				
144Nd	pPLCG2	K86-689.37	Fluidigm	0.33x
150Nd	pSTAT5	47	Fluidigm	1x
152Sm	pAKT	D9E	Fluidigm	0.33x
153Eu	pSTAT1	58D6	Fluidigm	0.33x
154Sm	pBtk/Itk	24a/BTK	BD Biosciences	0.5 µg/ml
156Gd	p38 [T180/Y182]	D3F9	Fluidigm	0.109x
158Gd	pSTAT3	4/P-Stat3	Fluidigm	1x
159Tb	pMAPKAPK2	27B7	Fluidigm	0.109x
162Dy	pLCK	4/LCK-Y505	Fluidigm	0.33x
164Dy	IkBa	L35A5	Fluidigm	0.33x
165Ho	pCREB	87G3	Fluidigm	0.033x
166Er	pNFKB	K10-895.12.50	Fluidigm	0.054x
167Er	pERK	D13.14.4E	Fluidigm	0.1x
171Yb	pZAP70	17a	Fluidigm	1x

Extended Data Table 1. Antibody panels for surface and intracellular staining.

	Healthy Control	Moderate COVID19	Severe COVID19
n	18	20	43
Age (years, mean+/-SD)	52.5+/-10.8	55.6+/-14.6	60.2+/-18.4
Female (n (%))	12 (66.7)	8 (40.0)	21 (48.8)
Race/Ethnicity (n(%))			
White	11 (61.1)	3 (15.0)	11 (25.6)
Black	5 (27.8)	17 (85.0)	32 (74.4)
Asian	1 (5.6)	0	0
Hispanic	1 (5.6)	0	0
Length of Stay (days, mean+/-SD)		5.7+/-4.0	17.9+/-10.1
Days of Symptoms at hospitalization (mean+/-SD)		9.0+/-11.2	6.7+/-6.6
Hospital Day of Sample (mean+/-SD)		0.5+/-1.1	2.1+/-2.9
ICU (n (%))		0	40 (93.0)
Mechanical Ventilation (n(%))		0	25 (58.1)
Mortality (n,(%))		0	16 (37)

Extended Data Table 2. Cohort Demographics and Description

		Moderate COVID19			Severe COVID19			
Analyte	Reference Range	Mean	Std. Dev	N	Mean	Std. Dev	N	p-value
ALANINE AMINOTRANSFERASE (Units/L)	7-55	52.89	75.19	19.00	66.81	83.14	26.00	5.42E-01
ALBUMIN (g/dL)	3.5-5	3.39	0.96	19.00	3.02	0.67	26.00	8.21E-03
ALKALINE PHOSPHATASE (Units/L)	40-130	79.37	53.68	19.00	113.35	146.11	26.00	3.71E-01
ANION GAP (mmol/L)	2-15	10.17	3.56	23.00	10.10	3.20	30.00	4.83E-01
ASPARTATE AMINOTRANSFERASE (Units/L)	10-50	60.11	65.84	19.00	151.81	399.47	26.00	3.28E-01
BASOPHIL ABSOLUTE (K/cumm)	0-0.1	0.03	0.06	18.00	0.02	0.05	26.00	5.09E-01
BASOPHIL PERCENT (%)	Not reported	0.38	0.28	18.00	0.22	0.16	26.00	2.05E-02
BILIRUBIN, TOTAL (mg/dL)	0.1-1.2	0.57	0.33	18.00	0.74	0.99	25.00	5.87E-01
CALCIUM, TOTAL (mg/dL)	8.5-10.3	8.51	1.94	23.00	8.61	0.80	30.00	3.25E-03
CHLORIDE (mmol/L)	97-110	95.04	21.26	23.00	104.77	7.50	30.00	2.61E-03
CO2, TOTAL (mmol/L)	22-32	25.17	6.12	23.00	24.63	4.85	30.00	2.43E-01
CREATININE (mg/dL)	0.8-1.3	1.52	1.42	23.00	1.70	1.53	40.00	8.14E-01
EOSINOPHIL PERCENT (%)	Not reported	0.81	1.21	18.00	0.56	0.96	28.00	3.97E-01
GLUCOSE (mg/dL)	70-199	129.17	65.37	23.00	144.30	46.85	30.00	1.54E-01
HEMATOCRIT (%)	38.9-50.3	34.85	10.04	23.00	33.49	6.36	30.00	8.66E-02
HEMOGLOBIN (g/dL)	13-17.5	11.22	3.38	23.00	10.77	2.07	30.00	1.24E-01
IMMATURE GRANULOCYTE ABSOLUTE (K/cumm)	0-0.1	0.09	0.23	19.00	0.16	0.32	28.00	2.33E-01
IMMATURE GRANULOCYTE PERCENT (%)	Not reported	0.81	0.70	17.00	1.29	1.91	26.00	9.90E-01
LYMPHOCYTE ABSOLUTE (K/cumm)	0.8-3.3	1.23	0.62	19.00	1.09	0.40	28.00	1.15E-01
LYMPHOCYTE PERCENT (%)	Not reported	18.41	9.43	19.00	13.43	8.82	28.00	2.44E-02
MEAN CELLULAR HEMOGLOBIN (pg)	27.1-33.3	26.70	6.60	23.00	28.15	2.87	30.00	8.75E-01
MEAN CELLULAR HEMOGLOBIN CONCENTRATION (g/dL)	32.3-35.7	30.73	6.97	23.00	32.17	1.49	30.00	6.77E-01
MEAN CELLULAR VOLUME (fL)	81.3-96.4	83.03	19.74	23.00	87.48	7.59	30.00	9.48E-01
MEAN PLATELET VOLUME (fL)	9.1-12.3	10.47	2.62	23.00	10.49	1.05	30.00	1.85E-01
MONOCYTE ABSOLUTE (K/cumm)	0.2-0.8	0.70	0.65	19.00	0.66	0.41	28.00	9.93E-01
MONOCYTE PERCENT (%)	Not reported	9.01	5.25	19.00	6.56	4.30	28.00	1.70E-02
NEUTROPHIL ABSOLUTE (K/cumm)	1.7-6.5	5.78	7.06	19.00	9.39	6.33	28.00	3.90E-03
NEUTROPHIL PERCENT (%)	Not reported	64.96	18.98	19.00	78.04	10.76	28.00	9.64E-03
NUCLEATED RBC ABS, AUTO (K/cumm)	0-0.01	0.00	0.01	23.00	0.02	0.05	30.00	1.05E-01
PLATELET (K/cumm)	150-400	198.00	68.42	23.00	268.53	156.49	40.00	4.23E-01
POTASSIUM, PLASMA (mmol/L)	3.3-4.9	3.81	0.99	23.00	4.30	0.61	30.00	4.60E-02
PROTEIN, TOTAL, PLASMA (g/dL)	6.5-8.5	7.22	1.86	19.00	6.98	1.05	26.00	2.96E-02
RED BLOOD CELL (M/cumm)	4.3-5.8	4.08	1.34	23.00	3.85	0.80	30.00	1.22E-01
RED CELL DISTRIBUTION WIDTH CV (%)	11.1-14.9	14.31	3.58	23.00	15.62	2.40	30.00	3.74E-01
RED CELL DISTRIBUTION WIDTH SD (fL)	35.7-48.1	44.97	11.89	23.00	49.37	6.52	30.00	2.21E-01
SODIUM (mmol/L)	135-145	130.39	28.77	23.00	139.50	7.29	30.00	1.96E-01
UREA NITROGEN SERUM (mg/dL)	8-25	22.00	20.13	23.00	28.68	21.05	40.00	1.02E-01
WHITE BLOOD CELL COUNT (K/cumm)	3.8-9.9	7.24	7.21	23.00	11.61	6.43	40.00	8.16E-04
MAGNESIUM (mg/dL)	1.4-2.5	1.76	0.67	14.00	2.17	0.26	26.00	9.54E-02
D-DIMER (ng/mL FEU)	<=499	1471.25	1485.83	16.00	8835.12	14601.13	33.00	2.13E-02
FERRITIN (ng/mL)	30-400	724.00	832.48	12.00	1585.82	2169.97	28.00	1.19E-01
INTERNATIONAL NORMALIZED RATIO ()	0.9-1.1	1.15	0.49	13.00	1.36	0.24	28.00	2.01E-02
CREATINE KINASE, TOTAL (Units/L)	30-200	331.80	514.94	5.00	1438.38	1270.83	8.00	8.94E-02
C REACTIVE PROTEIN (mg/L)	<=10	77.50	63.81	15.00	172.62	125.42	31.00	2.26E-02
LACTATE DEHYDROGENASE, TOTAL (Units/L)	100-250	294.60	142.38	10.00	597.76	365.50	17.00	1.90E-02
ERYTHROCYTE SEDIMENTATION RATE (mm/hr)	1-20	41.20	40.76	5.00	58.13	38.28	8.00	6.09E-01

Extended Data Table 3. Clinical Lab Data.

Feature	Healthy Donor*	Moderate COVID19*	Severe COVID19*	P value	q value	Discovery? (1% FDR)
PMN_pLCK	0.95+/-0.33	1+/-0.12	0.93+/-0.09	0.07	0.07	No
PMN_IkBa	0.98+/-0.08	1+/-0.1	0.99+/-0.07	0.94	0.58	No
PMN_pNKFb	1.05+/-0.19	1.06+/-0.1	1.11+/-0.2	0.18	0.15	No
PMN_pERK	1+/-0.01	1.01+/-0.01	1.04+/-0.05	0.00	0.00	Yes
PMN_pSTAT1	1+/-0.04	1.03+/-0.06	1.07+/-0.11	0.00	0.00	Yes
PMN_p38	1.24+/-0.47	1.03+/-0.06	1.04+/-0.09	0.47	0.31	No
PMN_pSTAT3	0.91+/-0.15	1.44+/-1.11	1.52+/-0.9	0.06	0.06	No
PMN_pCREB	1.04+/-0.13	0.99+/-0.06	1.03+/-0.17	0.33	0.24	No
PMN_PLCG2	1.01+/-0.01	1+/-0.02	1.01+/-0.02	0.26	0.20	No
PMN_pSTAT5	1.03+/-0.34	1.04+/-0.27	1.11+/-0.27	0.24	0.19	No
PMN_pAKT	0.99+/-0.01	1+/-0.02	1.01+/-0.02	0.02	0.02	No
PMN_pBtk/Itk	0.65+/-0.3	0.91+/-0.31	0.91+/-0.25	0.02	0.02	No
PMN_pMAPKAP2	1+/-0.03	1.02+/-0.04	1.07+/-0.17	0.15	0.13	No
PMN_pZAP70	1+/-0.02	1.01+/-0.03	1+/-0.03	0.99	0.61	No
PMN_pSTAT4	1.16+/-0.52	1.09+/-0.29	1.14+/-0.3	0.46	0.31	No
Mono_pLCK	1.12+/-0.11	1.05+/-0.1	0.98+/-0.07	0.00	0.00	Yes
Mono_IkBa	1.01+/-0.06	1.04+/-0.1	1.02+/-0.19	0.28	0.21	No
Mono_pNKFb	1.14+/-0.55	1.13+/-0.17	1.26+/-0.37	0.12	0.11	No
Mono_pERK	1+/-0.01	1.04+/-0.04	1.11+/-0.13	0.00	0.00	Yes
Mono_pSTAT1	1.04+/-0.07	1.08+/-0.12	1.21+/-0.32	0.05	0.06	No
Mono_p38	1.11+/-0.39	1.18+/-0.28	1.27+/-0.47	0.17	0.14	No
Mono_pSTAT3	1.31+/-0.39	2.3+/-1.37	3.24+/-2.17	0.00	0.00	Yes
Mono_pCREB	1.02+/-0.11	1.22+/-0.16	1.54+/-0.74	0.00	0.00	Yes
Mono_PLCG2	1.03+/-0.05	1+/-0.01	1.03+/-0.06	0.70	0.45	No
Mono_pSTAT5	1.44+/-0.95	0.99+/-0.25	1.31+/-0.61	0.24	0.19	No
Mono_pAKT	1.02+/-0.05	1+/-0.02	1.02+/-0.05	0.59	0.38	No
Mono_pBtk/Itk	0.87+/-0.3	0.95+/-0.07	1.01+/-0.2	0.08	0.08	No
Mono_pMAPKAP2	0.99+/-0.06	1.19+/-0.25	1.66+/-1.11	0.00	0.00	Yes
Mono_pZAP70	1.01+/-0.04	1+/-0.03	1.02+/-0.06	0.20	0.16	No
Mono_pSTAT4	1.01+/-0.35	0.95+/-0.27	1.08+/-0.26	0.09	0.09	No
CD4_pLCK	1.01+/-0.01	1.01+/-0.01	1.01+/-0.02	0.38	0.27	No
CD4_IkBa	1.01+/-0.04	1.02+/-0.09	1.14+/-0.26	0.00	0.01	Yes
CD4_pNKFb	1.25+/-0.48	1.03+/-0.22	1.02+/-0.29	0.54	0.36	No
CD4_pERK	1+/-0.01	1+/-0.01	1+/-0.01	0.08	0.08	No
CD4_pSTAT1	1.01+/-0.01	1.04+/-0.05	1.14+/-0.16	0.00	0.00	Yes
CD4_p38	1.1+/-0.3	1.06+/-0.12	1+/-0.1	0.45	0.31	No
CD4_pSTAT3	1.3+/-0.34	3.97+/-2.68	7.7+/-3.64	0.00	0.00	Yes
CD4_pCREB	1.02+/-0.04	1.09+/-0.08	1.17+/-0.23	0.00	0.00	Yes
CD4_PLCG2	1.01+/-0.01	1.01+/-0.01	1.02+/-0.03	0.54	0.36	No
CD4_pSTAT5	1.02+/-0.15	0.93+/-0.27	1.06+/-0.3	0.09	0.08	No
CD4_pAKT	1.01+/-0.01	1.01+/-0.02	1.02+/-0.03	0.02	0.02	No
CD4_pBtk/Itk	0.83+/-0.16	0.97+/-0.05	1.01+/-0.11	0.00	0.00	Yes
CD4_pMAPKAP2	1.02+/-0.04	1.12+/-0.2	1.3+/-0.53	0.00	0.00	Yes
CD4_pZAP70	1.02+/-0.05	1.03+/-0.06	1.05+/-0.07	0.19	0.15	No
CD4_pSTAT4	0.99+/-0.2	1.11+/-0.23	1.17+/-0.2	0.01	0.01	No
CD8_pLCK	1.01+/-0.02	1.01+/-0.01	1.02+/-0.02	0.77	0.49	No
CD8_IkBa	1+/-0.04	1.02+/-0.09	1.09+/-0.18	0.01	0.01	Yes
CD8_pNKFb	1.51+/-0.7	1.13+/-0.2	1.17+/-0.35	0.42	0.30	No
CD8_pERK	1+/-0.03	0.99+/-0.03	1.01+/-0.03	0.02	0.02	No
CD8_pSTAT1	1.01+/-0.01	1.03+/-0.04	1.08+/-0.11	0.00	0.00	Yes
CD8_p38	1.18+/-0.43	1.11+/-0.2	1.01+/-0.12	0.26	0.20	No
CD8_pSTAT3	1.17+/-0.25	2.23+/-1.04	3.46+/-1.97	0.00	0.00	Yes
CD8_pCREB	1.05+/-0.04	1.11+/-0.1	1.23+/-0.29	0.00	0.00	Yes

CD8_PLCG2	1+/-0	1+/-0	1.01+/-0.02	0.00	0.00	Yes
CD8_pSTAT5	1.09+/-0.15	0.94+/-0.23	1.03+/-0.22	0.01	0.02	No
CD8_pAKT	1.01+/-0.01	1.01+/-0.01	1.02+/-0.03	0.26	0.20	No
CD8_pBtk/Itk	0.81+/-0.16	0.95+/-0.05	0.98+/-0.08	0.00	0.00	Yes
CD8_pMAPKAP2	1.02+/-0.04	1.1+/-0.18	1.25+/-0.45	0.00	0.00	Yes
CD8_pZAP70	1.01+/-0.04	1.02+/-0.07	1.03+/-0.06	0.14	0.12	No
CD8_pSTAT4	0.94+/-0.17	1.02+/-0.17	1.06+/-0.16	0.03	0.03	No
NK_pLCK	1.01+/-0.07	0.98+/-0.05	1.03+/-0.08	0.02	0.03	No
NK_IkBa	1.03+/-0.04	1.04+/-0.1	1.16+/-0.22	0.01	0.01	Yes
NK_pNKFb	1.32+/-0.65	1.02+/-0.17	0.96+/-0.26	0.13	0.11	No
NK_pERK	1+/-0.01	1+/-0.01	1.03+/-0.04	0.00	0.00	Yes
NK_pSTAT1	1.01+/-0.02	1.02+/-0.03	1.06+/-0.06	0.00	0.00	Yes
NK_p38	1.17+/-0.51	1.13+/-0.28	1.03+/-0.24	0.37	0.26	No
NK_pSTAT3	1.15+/-0.25	1.48+/-0.34	1.98+/-0.79	0.00	0.00	Yes
NK_pCREB	1.02+/-0.05	1.08+/-0.09	1.26+/-0.35	0.00	0.00	Yes
NK_PLCG2	1+/-0.01	1+/-0	1.02+/-0.05	0.09	0.08	No
NK_pSTAT5	1.16+/-0.21	1.06+/-0.25	1.4+/-0.65	0.07	0.07	No
NK_pAKT	1+/-0.01	1.01+/-0.01	1.03+/-0.04	0.00	0.00	Yes
NK_pBtk/Itk	0.83+/-0.17	0.95+/-0.04	1.02+/-0.14	0.00	0.00	Yes
NK_pMAPKAP2	1.02+/-0.03	1.07+/-0.07	1.26+/-0.39	0.00	0.00	Yes
NK_pZAP70	1+/-0.02	1+/-0.01	1.02+/-0.04	0.07	0.07	No
NK_pSTAT4	1.1+/-0.27	1.17+/-0.2	1.31+/-0.31	0.03	0.03	No
PMN_CD16	0.76+/-0.2	1+/-0.65	0.84+/-0.53	0.63	0.41	No
PMN_CD11b	0.96+/-0.42	0.93+/-0.25	0.72+/-0.23	0.01	0.01	Yes
PMN_CD66b	0.98+/-0.2	1.13+/-0.28	0.99+/-0.36	0.06	0.07	No
PMN_CD33	1.38+/-1.22	1.05+/-0.85	1.02+/-0.74	0.97	0.60	No
PMN_CD11c	1.24+/-0.52	1.86+/-1.14	1.41+/-0.73	0.10	0.09	No
PMN_CD15	1.2+/-0.33	0.85+/-0.28	0.81+/-0.36	0.00	0.00	Yes
PMN_HLA-DR	1.13+/-0.2	0.91+/-0.21	0.87+/-0.32	0.00	0.00	Yes
Mono_CD11b	1.18+/-0.23	0.97+/-0.28	0.77+/-0.23	0.00	0.00	Yes
Mono_CD14	0.88+/-0.1	0.86+/-0.19	0.66+/-0.23	0.00	0.00	Yes
Mono_CD33	1.45+/-0.7	1.01+/-0.31	0.86+/-0.32	0.00	0.00	Yes
Mono_HLA-DR	0.53+/-0.23	0.4+/-0.29	0.36+/-0.29	0.01	0.01	Yes
B cells	1.94+/-1.02	2.17+/-1.85	1.81+/-1.64	0.44	0.30	No
basophils	0.6+/-0.29	0.36+/-0.43	0.15+/-0.13	0.00	0.00	Yes
classical monocytes	5.81+/-1.7	3.84+/-3.14	2.82+/-2.63	0.00	0.00	Yes
pDC	0.12+/-0.1	0.07+/-0.1	0.04+/-0.04	0.00	0.00	Yes
NK cells	2.92+/-1.57	2.73+/-1.84	1.45+/-1.29	0.00	0.00	Yes
NKT cells	0.66+/-0.88	1.15+/-0.94	0.74+/-1.29	0.03	0.03	No
T cells	18.06+/-3.72	15.56+/-9.16	6.94+/-5.09	0.00	0.00	Yes
CD4 T cells	11.61+/-3.23	9.28+/-5.68	4.78+/-3.61	0.00	0.00	Yes
CD8 T cells	3.91+/-2.65	4.99+/-4.18	1.6+/-1.53	0.00	0.00	Yes
Neutrophils	65.37+/-4.18	72.38+/-13.17	81.89+/-11.26	0.00	0.00	Yes

Extended Data Table 4. Immunologic Features Defined by CyTOF. * data presented as mean+/-StDev. P values calculated by Kruskall-Wallis ANOVA. Q values calculated by Benjamini, Krieger and Yekutieli for False Discovery Rate (FDR) of 1%.

Soluble Marker	Healthy Donor (n=18; Mean+/- SD)	Moderate COVID19 (n=15; Mean+/-SD)	Severe COVID19 (n=21; Mean+/-SD)	P value (Kruskal-Wallis)	q value (Benjamini, Krieger and	Discovery? (1%FDR)	Hierarchial Clustering
IL-6	2.31+/-1.99	32.79+/-52.3	249.78+/-226.05	3.25E-08	9.20E-07	**Yes**	Cluster A
MCP-1	445.87+/-156.23	805.73+/-1023.88	1225.79+/-916.06	1.97E-03	7.97E-03	**Yes**	Cluster A
HGF	40.76+/-23.07	213.33+/-373.2	1595.74+/-2208.43	1.09E-07	1.03E-06	**Yes**	Cluster A
IL-1RA	33.32+/-10.4	165.23+/-120.27	229.59+/-158.55	2.21E-07	1.56E-06	**Yes**	Cluster A
IP-10	29.14+/-36.49	108.02+/-80.71	228.79+/-193.5	7.67E-06	4.34E-05	**Yes**	Cluster A
IL-2R	47.09+/-36.7	149.08+/-217.33	167.1+/-161.18	8.55E-03	2.23E-02	No	Cluster A
MIG	28.31+/-30.23	50.6+/-56.72	138.61+/-101.41	3.83E-04	1.80E-03	**Yes**	Cluster A
IL-8	14.62+/-3.35	77.64+/-69.91	148.4+/-104.65	6.84E-08	9.67E-07	**Yes**	Cluster A
FGF-basic	12.23+/-13.46	10.42+/-11.38	15.02+/-14.16	1.79E-01	2.30E-01	No	Cluster B
IL-13	3.08+/-2.01	3.86+/-1.87	5.64+/-3.74	1.04E-02	2.45E-02	No	Cluster B
MIP-1b	61.18+/-38.38	100.14+/-84.9	112.86+/-94.99	2.20E-01	2.40E-01	No	Cluster B
IL-15	32.21+/-29.83	98+/-160.02	103.25+/-135.13	1.47E-01	2.08E-01	No	Cluster B
EGF	68.06+/-31.13	137.92+/-140.79	117.23+/-104.89	9.86E-02	1.55E-01	No	Cluster B
IL-1a	3.37+/-4.68	45.97+/-165.11	7.76+/-88.69	1.14E-01	1.70E-01	No	Cluster B
IFN-g	2.68+/-2.6	3.64+/-7.21	2.43+/-4.53	7.99E-01	6.46E-01	No	Cluster B
IFN-a	24.91+/-27	37.94+/-27.14	45.33+/-34.49	4.53E-02	8.55E-02	No	Cluster B
IL-3	18.63+/-19.2	46.75+/-76.94	36.6+/-54.91	5.05E-01	4.33E-01	No	Cluster B
IL-2	9.64+/-10.86	104.86+/-311.14	44.66+/-175.44	1.63E-01	2.19E-01	No	Cluster B
IL-4	3.27+/-3.25	7.54+/-16.36	6.87+/-10.46	2.54E-01	2.56E-01	No	Cluster B
IL-1b	0.76+/-0.57	3.93+/-7.92	3.17+/-4.97	4.63E-03	1.64E-02	No	Cluster C
G-CSF	25.79+/-18.03	21.66+/-27.13	23.42+/-24.79	2.07E-01	2.40E-01	No	Cluster C
RANTES	1148.9+/-985.82	1192.94+/-860.78	2154.6+/-2986.73	5.61E-01	4.66E-01	No	Cluster C
IL-17A	4.56+/-4.86	12.53+/-29.86	3.83+/-17.28	8.60E-02	1.43E-01	No	Cluster C
VEGF	2.6+/-3.07	18.54+/-30.42	5.5+/-17.51	1.28E-02	2.70E-02	No	Cluster C
IL-17F	77.84+/-82.63	702.56+/-2092.1	205.97+/-1148.7	2.06E-01	2.40E-01	No	Cluster C
IL-9	1.77+/-3.03	51.49+/-126.37	4.75+/-70.12	3.31E-01	3.02E-01	No	Cluster C
TNFa	2.21+/-5.19	31+/-99.88	3.05+/-54.02	7.39E-03	2.23E-02	No	Cluster C
IL-10	30.87+/-58.67	15.22+/-13.37	55.86+/-65.32	1.34E-02	2.70E-02	No	Cluster D
IL-12	46.64+/-22.84	108.85+/-165.34	61.2+/-93.65	2.65E-01	2.56E-01	No	Cluster D
EOTAXIN	98.61+/-66.09	79.26+/-105.11	57.74+/-74.32	7.91E-02	1.40E-01	No	Cluster D
MIP-1a	2.05+/-4.18	10.27+/-21.84	38.83+/-67.18	8.66E-03	2.23E-02	No	Cluster D
GM-CSF	2.8+/-6.2	4.42+/-10.04	2.57+/-6.5	3.47E-01	3.06E-01	No	Cluster D
IL-5	2.12+/-2.16	2.09+/-3.18	6.94+/-13.12	2.44E-01	2.56E-01	No	Cluster D
IL-7	20.29+/-23.55	6.05+/-4.38	21.58+/-29.78	2.72E-01	2.56E-01	No	Cluster D
IL-22	42.17+/-33.71	38.37+/-54.47	53.63+/-47.32	2.13E-01	2.40E-01	No	Cluster D

Extended Data Table 5. Cytokines Levels.